REPORT DOCUMENTATION PAGE

Public reporting burden for this collection of information is estimated to average 1 hour per response, including the time for re
data needed, and completing and reviewing this collection of information. Send comments regarding this burden estimate or ↲
this burden to Department of Defense, Washington Headquarters Services, Directorate for Information Operations and Reports (0704-0188), 1215 Jefferson Davis Highway, Suite 1204, Arlington, VA 22
4302. Respondents should be aware that notwithstanding any other provision of law, no person shall be subject to any penalty for failing to comply with a collection of information if it does not display a c
valid OMB control number. **PLEASE DO NOT RETURN YOUR FORM TO THE ABOVE ADDRESS.**

1. REPORT DATE (12-02-2008)	2. REPORT TYPE Final	3. DATES COVERED (From - To) 04/15/2007-11/30/2007

4. TITLE AND SUBTITLE

Modeling of Flow about Pitching and Plunging Airfoil Using High-order Schemes

5a. CONTRACT NUMBER

5b. GRANT NUMBER
FA9550-07-1-0314

5c. PROGRAM ELEMENT NUMBER

6. AUTHOR(S)
PI Povitsky, graduate student Gopalan

5d. PROJECT NUMBER

5e. TASK NUMBER

5f. WORK UNIT NUMBER

7. PERFORMING ORGANIZATION NAME(S) AND ADDRESS(ES)

The University of Akron   The University of Akron, Akron, OH, USA

8. PERFORMING ORGANIZATION REP(NUMBER

9. SPONSORING / MONITORING AGENCY NAME(S) AND ADDRESS(ES)
AFOSR
875 N Randolph St
Arlington VA 22203
Rhett Jeffries/NA

10. SPONSOR/MONITOR'S ACRONYM(
John. D. Schmiseur

11. SPONSOR/MONITOR'S REPORT NUMBER(S)

12. DISTRIBUTION / AVAILABILITY STATEMENT

Distribution Statement A: Approved for public release. Distribution is unlimited.

13. SUPPLEMENTARY NOTES

20080331079

14. ABSTRACT A high-order non-uniform compact finite-difference algorithm with numerical filtering and low storage Runga-Kutta scheme is developed to perform numerical simulations on orthogonal grids generated about plunging and pitching airfoils. The grids, which move with the pitching and plunging airfoil, are generated using "Streamfunction as a coordinate approach" (SFC). SFC is widely used in combination with lower-order schemes in Computational Fluid Dynamics. The straightforward implementation of SFC create rather coarse grid at the vicinity of stagnation points that smears high-order numerical computations of aeroacoustics and unsteady aerodynamics. To improve the solution accuracy, non-uniform SFC grid with appropriate grid stretching and filtering of solution is implemented. The different kinds of SFC grid generation methods and the grid clustering in the vicinity of stagnation point are discussed. The applications of the developed grid generator and numerical solver to problems based on linearized Euler equations, for which analytical solutions are available, are shown first. Then, the methodology is applied to unsteady aerodynamics of pitching and plunging airfoils. The application of the developed grid generator and numerical solver to plunging airfoil problems are discussed and compared with available experimental data including lift force for plunging NACA0012 airfoil and visualization of vortical flowfield for plunging SD7003 airfoil. Finally, the use of flapping airfoil for control of gust-induced oscillations of airfoil lift force is discussed.

Personnel supported: PI Prof. Alex Povitsky, graduate student Harish Gopalan

Publications pertinent to the grant from the beginning of grant in April 2007:

1. H. Gopalan and A. Povitsky, Streamfunction-Potential Function Coordinates for Aeroacoustics and Unsteady Aerodynamics, submitted to AIAA Journal, December 2007.
2. H. Gopalan and A. Povitsky, Streamfunction-Potential function coordinates in computational aeroacoustics, the 37th AIAA Fluid Dynamics Conference, AIAA Paper 2007-4108, June 2007.
3. H. Gopalan, A. Povitsky and M. Ol, A Numerical Study of Gust Suppression by Flapping Airfoils, submitted to the 26th AIAA Applied Aerodynamics Conference, Honolulu, HW, 2008.
4. T. Zheng, G. Vatistas and A. Povitsky, Sound Generation by Street of Vortices in a Non-uniform Flow, Physics of Fluids, Vol. 19, 037103, 2007.
5. T. Zheng, A. Povitsky, and G. Vatistas, Vortex-generated Sound in Flow about Spinning Cylinders, Journal of Computational Acoustics, Vol. 16, No. 4, 2008, to appear.

Nomenclature

U = Solution vector
E, F = Fluxes
u, v = Cartesian velocity components
ρ = Density
p = Pressure
e = Internal energy
E_t = Total energy
$\tau_{xx}, \tau_{xy}, \tau_{yy}$ = Shear stress components
q_x, q_y = Heat Flux
Re = Reynolds number
Pr = Prandtl number
M = Mach number
T = Temperature
(x, y) = Cartesian coordinates
(ψ, φ) = Streamfunction-potential function coordinates
J = Jacobian
$(x_\varphi, x_\psi ...)$ = Grid metrics
(x_t, y_t) = Grid speed
δ_ψ = location of the first grid line above the wall
σ_i = Strength of vortices
τ = Clustering parameter in φ direction
P, Q = Clustering parameters in ψ direction
θ = Angle between grid lines
g = Metric tensor
St = Strouhal number

I. Introduction

Von Mises (Ref. 1) was the first to introduce streamfunction as a coordinate (SFC). In his study, he used the streamfunction as the coordinate across boundary layer while the transverse Cartesian coordinate was unchanged. A limitation of this approach is the degeneracy of the grid[2] near the leading edge of the airfoil. A number of modifications have been proposed to deal with this issue[2-5]. The advantage of the SFC methodology in CFD lies in the fact that the streamfunction serves both the purpose of grid generation and description of motion for steady flows. The SFC approach has found applications in a wide variety of fields including two-dimensional channel design[6,7], nozzle inverse flow design

problem[8],inverse design of aerodynamic shapes[9,10] and turbomachinery flows, to name a few. In the aerodynamics of moving airfoils, the generated SFC grid can move with the airfoil and keep the boundary layer well-resolved. This feature is crucial for accurate modeling of flow separation.

SFC allows for the use of economic single-grid high-order finite-difference type schemes for complex geometry. In terms of computational time per grid point, this method is advantageous compare to multiple grids or unstructured grids combined with high-order schemes and interface matching conditions. Although the SFC is widely used in combination with lower-order numerical schemes in CFD, the straightforward implementation of SFC create rather coarse grid at the vicinity of stagnation points that smears high-order numerical computations of aeroacoustics and unsteady aerodynamics of flapping airfoils. The application of the SFC methodology for numerical computations with high-order of approximation is considered in the present report.

Though the main application of SFC was in the field of inverse flow device design, it has found application in other fields too. Finnigan (Ref.11-13) used the SFC approach to study turbulent shear flows and chaotic systems. The method has also found application in the field of two-phase flows[14] and flow through porous media[15].Chakravarthy[16] used the streamlines and potential lines of an incompressible solution to generate a grid for transonic nozzle flow. Adamczyk[17] generated O-type, C-type and split conformal grids for turbomachinery flows using an integral formulation similar to the Symm construction[18] to generate orthogonal grids.

The streamfunctions are defined only for two-dimensional flows; nevertheless, applications can be found in literature where the SFC has been applied to 3-D problems. Anderson[19] generated a three-dimensional coordinate system by rotating an axisymmetric 2-D duct about its axis. Briley[20] produced the grid for a 3-D duct by stacking 2-D systems. Hounjet [21, 22] generated 2-D and 3-D grids using the panel method solution of the velocity potential. The method was used to generate O-type and multi-block OH-type grids about transverse cross-sections of transport type aircrafts. As opposed to O-grids and C-grids,

the SFC coincides with Cartesian coordinates in the far-field that makes straightforward the use of outflow boundary conditions.

The problem with the SFC is that a uniform distribution of grid points in the computational domain produces coarse cells close to the stagnation point. For the only velocity scale in the computational set-up, the velocity is slow at the vicinity of stagnation point and the coarse grid does not introduce significant error. However, this problem is critical for unsteady aerodynamics including flapping airfoils because of the presence of another velocity scale such as speed of moving airfoil. Indeed the speed of moving airfoil is large for higher frequency of airfoil pitching and plunging. The error introduced by coarse grid may harm the effort to apply high-order schemes to problems of flapping airfoils.

To circumvent this issue, the following combination of algorithmic steps has been implemented in the current study. A hyperbolic stretching function[23] was used for grid refinement close to the solid boundaries. The degree of stretching will be chosen carefully to make sure that the grid does not become extremely coarse in the far field. The spatial differencing is performed using a non uniform compact scheme[24, 25]. To remove the oscillations due to the grid non-uniformity, an implicit Pade-type filter[26] is employed in the current study. The explicit time marching is performed using a Runga-Kutta algorithm, implemented in the low-storage form[27]. A simple energy transfer and annihilation method[28] is used at the domain boundaries for absorbing the outgoing energy.

The governing equations are listed in Sec.2. Sec.3 discusses the SFC method. The numerical algorithm is discussed in Sec. 4.Numerical results are discussed in Sec.5. In Sec. 6, gust suppression by plunging airfoil is described. Conclusions are drawn in Sec 7.

II. Governing Equations

The governing equations are the 2-D compressible Navier-Stokes equations. To keep the formulation applicable to unsteady aerodynamics of flapping airfoils, the Navier-Stokes equations are cast in moving grid[30].

$$\frac{\partial U}{\partial t} + \frac{\partial E}{\partial x} + \frac{\partial F}{\partial y} = 0 \tag{1}$$

On introducing a transformation $(x,y,t) \rightarrow (\varphi(x,y,t), \psi(x,y,t), \tau)$, the governing Navier-Stokes equations become

$$\frac{\partial U}{\partial \tau} + \frac{\partial \phi}{\partial t}\frac{\partial U}{\partial \phi} + \frac{\partial \psi}{\partial t}\frac{\partial U}{\partial \psi} + \frac{\partial \phi}{\partial x}\frac{\partial E}{\partial \phi} + \frac{\partial \psi}{\partial x}\frac{\partial E}{\partial \psi} + \frac{\partial \phi}{\partial y}\frac{\partial F}{\partial \phi} + \frac{\partial \psi}{\partial y}\frac{\partial F}{\partial \psi} = S(t) \tag{2}$$

where U denotes the solution vector, E and F are the fluxes (includes both the inviscid and viscous flux components) and (φ, ψ) denotes the potential function and streamfunction respectively. S (t) refers to acoustic or vortical sources of sound that are presented in the flow.

The solution vector and the flux components are given by

$$U = \begin{bmatrix} \rho \\ \rho u \\ \rho v \\ E_t \end{bmatrix} \tag{3}$$

$$E = \begin{bmatrix} \rho u \\ \rho u^2 + p - \tau_{xx} \\ \rho u v - \tau_{xy} \\ (E_t + p)u - u\tau_{xx} - v\tau_{xy} + q_x \end{bmatrix} \tag{4}$$

3/13/2008

$$F = \begin{bmatrix} \rho v \\ \rho uv - \tau_{xy} \\ \rho v^2 + p - \tau_{yy} \\ (E_t + p)u - u\tau_{xy} - v\tau_{yy} + q_y \end{bmatrix} \qquad (5)$$

And

$$E_t = \rho(e + 0.5(u^2 + v^2)) \qquad (6)$$

The shear stresses and the heat flux vector are given by

$$\tau_{xx} = \frac{2}{3\,\mathrm{Re}}(2\frac{\partial u}{\partial x} - \frac{\partial v}{\partial y}) \qquad (7)$$

$$\tau_{yy} = \frac{2}{3\,\mathrm{Re}}(2\frac{\partial v}{\partial y} - \frac{\partial u}{\partial x}) \qquad (8)$$

$$\tau_{xy} = \frac{1}{\mathrm{Re}}(2\frac{\partial u}{\partial y} + \frac{\partial v}{\partial x}) \qquad (9)$$

$$q_x = \frac{-1}{(\gamma - 1)M\,\mathrm{Re}\,\mathrm{Pr}}\frac{\partial T}{\partial x} \qquad (10)$$

$$q_y = \frac{-1}{(\gamma - 1)M\,\mathrm{Re}\,\mathrm{Pr}}\frac{\partial T}{\partial y} \qquad (11)$$

where Re, M, Pr are the Reynolds number, Mach number and Prandtl number. The equations of state for ideal gas become

$$p = (\gamma - 1)\rho e \qquad (12)$$

$$T = \frac{\gamma M^2 p}{\rho} \qquad (13)$$

The grid metrics are calculated using the following equations

$$\frac{\partial \phi}{\partial x} = J \frac{\partial y}{\partial \psi} \qquad (14)$$

$$\frac{\partial \phi}{\partial y} = -J \frac{\partial x}{\partial \psi} \qquad (15)$$

$$\frac{\partial \psi}{\partial x} = -J \frac{\partial y}{\partial \phi} \qquad (16)$$

$$\frac{\partial \psi}{\partial y} = J \frac{\partial x}{\partial \phi} \qquad (17)$$

$$\frac{\partial \phi}{\partial t} = -\frac{\partial x}{\partial \tau}\frac{\partial \phi}{\partial x} - \frac{\partial y}{\partial \tau}\frac{\partial \phi}{\partial y} \qquad (18)$$

$$\frac{\partial \psi}{\partial t} = -\frac{\partial x}{\partial \tau}\frac{\partial \phi}{\partial x} - \frac{\partial y}{\partial \tau}\frac{\partial \phi}{\partial y} \qquad (19)$$

where J is the Jacobian of the transformation which is given by $J = \frac{1}{(x_\phi y_\psi - x_\psi y_\phi)}$.The grid

velocities (x_τ, y_τ) are computed from analytical expression for the rigid body motion of the grid around

the moving body. The grid metrics are computed using the same high-order spatial discretization scheme

(see Section IV) used for the computation of the fluxes.

III. Grid Generation

Streamfunction and potential function are conjugate harmonic functions and are orthogonal to each other. This property can be utilized for the generation of orthogonal numerical conformal grids. This idea has been employed for 2D grid generation and in some cases extended for 3D problems. For simple geometries, analytical solutions can be constructed for streamfunction and potential function using elementary solutions of Laplace equation. For such geometries, the exact solution is a system of non-linear equations which can be inverted using Newton's method to obtain the values of the coordinates (x, y) when the values of streamfunction and potential function are specified. This method is referred in the current study as analytical grid generation. For problems, where the exact solution is not available, the numerical values of stream function and potential function on the solid body can be computed using panel methods. The numerical values of streamfunction and potential function on the solid body are used to distribute streamlines and potential lines in the numerical domain and an approximate system of non-linear equations for streamfunction and potential function can be inverted to obtain the coordinates (x,y). This method is referred as the numerical grid generating method. For problems involving multiple bodies in the domain, it is possible to generate the grid by applying the panel method for the system of bodies directly or by applying the panel method separately to each body and joining the separate grids using stitching.

Potential lines become coarse close to the stagnation points. For accurate numerical representation of the problem, this issue needs to be resolved. In the current study, a hyperbolic sine function is used to cluster the potential lines and it is found that the grid coarse elements close to the stagnation points can be removed. A hyperbolic tangent function is employed to cluster the streamlines for resolving the boundary layer.

A. Analytical Method

The analytical grid generating system is the faster of the two above-listed methods as it involves just a single step inversion of the non linear system of equations. The deviation from orthogonality for grids generated using the analytical method is negligible. The analytical grid generation method is implemented as follows:

- Construct the exact analytical solution for streamfunction and potential function.

- Generate the numerical domain between certain maximum and minimum values of streamfunction and potential function.

- Find (x, y) coordinates for any given grid point (ψ_i, φ_j). To achieve it, invert the non-linear system of equations using the Newton's method within a specified tolerance. For the left corner point a random initial guess is used. For rest of the grid points, the previous grid point was used as an initial guess.

- For boundary layer resolution, streamlines are clustered using the following formula: $\delta_\psi = \dfrac{1}{N\sqrt{Re}}$, where N is the number of points across the boundary layer and $\dfrac{1}{\sqrt{Re}}$ is the scale of thickness of the boundary layer.

An example of the grid generated using the above algorithm is considered for the case of uniform flow past a single cylinder (see Fig. 1a). For this case, the analytical expressions for streamfunction and potential function are given by

$$\phi = x(1 + \frac{R^2}{x^2 + y^2}) \qquad (20a)$$

$$\psi = y\left(1 - \frac{R^2}{x^2 + y^2}\right) \quad (20b)$$

As can be seen in Fig. 1a, the uniform grid obtained is coarse close to the stagnation point. The way of avoiding this is discussed in the section D.

B. Numerical Grid Generating System

The numerical grid generating system consists of two parts: i) apply a panel (boundary element method) solver to find the velocity the potential, and ii) invert an approximate numerical expression for streamfunction and potential function to find (x_i, y_j) coordinates for any given grid point (ϕ_i, ψ_j). The orthogonal property of the numerical method is comparable to the hyperbolic grid generating method with the advantage of being able to specify the outer boundary. The following algorithm is used for the numerical grid generation:

- Construct a panel method solution of the potential function on the solid boundary. In the current study, discrete potential vortices[31] are used as an elementary solution in panel methods. The panel method solves for the discrete potential vortex strengths σ_i at each boundary cell (panel).

- Since the surface of the body is a streamline, the ideal value of streamfunction will be constant on the surface of the body. The value of streamfunction on the surface of the body computed using the panel methods will have some numerical error from the computations. Hence the numerical value of the streamline will not be the same at all the points on the surface of the body. To account for this error, the values of the streamline on the body are

Final report FA9550-07-1-0314   3/13/2008

denoted as C_u and C_l where C_u is the maximum value of the streamline on the body and C_l is the minimum value of the streamline on the body.

- Next, the first streamline above and below the body are constructed as $\psi_1 = C_1 C_u$ and $\psi_{-1} = C_2 C_l$, where C_1, C_2 are used to ensure that the streamlines does not cross into the body. The values of C_1 and C_2 are set to 1.02 and 0.98 respectively. Further, to ensure that the required number of points is clustered in the boundary layer, the following condition is satisfied in the numerical algorithm: $\delta_\psi = |\psi_1 - \psi_{-1}|$, where $\delta_\psi = \dfrac{1}{N\sqrt{\mathrm{Re}}}$. The number of discrete vortices (panels) is increased on the surface of the solid body and the panel method is repeated until the above condition is satisfied.

- Generate the numerical domain between certain maximum and minimum values of streamfunction and potential function.

- The following system of equations is inverted to obtain the values of (x,y)

$$\phi(x,y) = x - \sum_{i=1}^{N} \frac{\sigma_i}{2\pi} \tan^{-1}\left(\frac{y-y_i}{x-x_i}\right) \tag{21a}$$

$$\psi(x,y) = y + \sum_{i=1}^{N} \frac{\sigma_i}{2\pi} \ln\left(\sqrt{(x-x_i)^2 + (y-y_i)^2}\right) \tag{21b}$$

An example of the application of the above method is shown for the case of a cambered airfoil (Fig.2). It can be seen that the grid lines are orthogonal to each other. The above grid generating algorithm has the ability to produce high quality orthogonal grids on different kinds of geometries (Fig.1-4).

Final report FA9550-07-1-0314   3/13/2008

Elliptic grid generating system can generate smooth grids but the implementing of boundary layer clustering and generating orthogonal grids require some effort. The hyperbolic grid generation can generate orthogonal grids but the outer boundary cannot be specified and the grid can deteriorate rapidly close to sharp edges unless grid lines are clustered or artificial dissipation is added. The current grid generation method can be viewed as a hybrid method which is able to achieve the orthogonality and grid clustering with the ability to specify the outer boundary at the same time. The implementation of grid clustering will be discussed in Sec.III.D.

C. Grid Stitching

For problems, involving multiple bodies like two wings in tandem or a combination of steady and unsteady wings, the panel method can be used to generate a single-block structured grid. An example is shown in Fig.3 for the generation of grids around two cylinders placed in tandem. The panel method grid generator can be used for inviscid studies but is not a convenient grid generator for viscous flows due to the lack of local grid control around each body. This becomes extremely important for studying flows with boundary layer resolution. To have more control on the grid about individual bodies stitching method is employed. In this method, the grids around each body are generated using either analytical or numerical grid generating system. The local grids are then stitched together at an interface (stitching boundary) [32]. In the current study, an elliptic grid generating method is used for stitching the two parts of the grid together to keep the procedure simple [32, 33]. The following steps are used for generating the patched grids:

- Generate the local streamfunction grid around each body.

- The region close to the patched area might have grid lines crossing each other. To remove those grid lines and make the grid smooth, the grid lines, which do not intersect at both the ends, are selected and fixed.

- For the top and bottom lines, the corners from the previous grid lines are used to distribute points on the corners using linear interpolation.

- Once the four corner grid lines are fixed, an elliptic grid generation method is used for smoothing the patched region.

The above steps ensure that the grid stitching is local and does not change the global grid. The size of the patching domain is problem-dependent and needs some trial and error. This approach has been applied in the current study to generate a single non-uniform structured grid around two cylinders in tandem. The grid is generated locally around each cylinder and is then smoothed using an elliptic grid generator. Grid generated by panel method around two cylinders in tandem is shown in Fig.4a. The grid generated by stitching is shown in Fig.4b. The grids are similar to each other if no clustering is implemented.

D. Grid Clustering

Vinokur[34] found that the hyperbolic sine functions are the best for concentrating points in the middle of domain and hyperbolic tangent function for clustering at the ends of domain. As can be seen from Fig.1a, the grid becomes coarse close to the stagnation point of the cylinder. Hence to remove the coarse grid cell in the φ direction, which is near stagnation points in the middle of the domain, a hyperbolic sine function is employed[35].

$$x = x_c(1 + \frac{\sinh(\tau(\eta - B))}{\sinh(\tau B)}) \qquad (22a)$$

3/13/2008

where x_c is the location in physical domain around which the grid clustering is required (stagnation points have $x_c = \pm 0.5$), η is the normalized computational coordinate which varies from 0 to 1. The clustering parameter τ varies from zero to infinity, where $\tau=0$ corresponds to a uniform grid (no clustering). The parameter B is given by

$$B = \frac{1}{2\tau} \ln \left[\frac{1+(e^\tau - 1)(x_c/h)}{1+(e^{-\tau}-1)(x_c/h)} \right] \qquad (22b)$$

where h is the length of physical domain in either positive or negative direction.

For problems involving viscous flows, resolution of boundary layers become very important. To cluster grid in the ψ direction in boundary layer the following approach is used[33]:

$$s = P\eta + (1-P)(1 - \frac{\tanh[Q(1-\eta)]}{\tanh(Q)}) \qquad (23a)$$

$$x = x_i + s(x_e - x_i) \qquad (23b)$$

The factors P and Q control the clustering and x_i and x_e are the limits of physical domain. The comparison between grid generated with the application of hyperbolic sine function (22) is shown in Fig.1b with a clustering parameter $\tau=5$. The clustering of points in the boundary layer for the SD 7003 airfoil is shown in Fig.2b with $P=0.1$ and $Q=4$ in Eq. (23), and $\tau=2.5$ in Eq. (22).

E. Orthogonality in 2D

The orthogonality property of the grid is measured by computing the angle between grid lines, which is given by

$$\theta = \cos^{-1}\left(\frac{g_{12}}{\sqrt{g_{11}g_{22}}}\right) \tag{24}$$

where g is the metric tensor which is calculated by

$$g_{ij} = \sum_{k=1}^{2}\left(\frac{\partial x_k}{\partial q_i}\right)\left(\frac{\partial x_k}{\partial q_j}\right) \tag{25}$$

where $(x_1, x_2) = (x, y)$ and $(q_1, q_2) = (\phi, \psi)$. For an orthogonal grid, θ should be equal to 90 degrees. The maximum measured deviation from orthogonality was around 4-5 degrees for both grids about the cylinder and airfoil. The deviation was observed only at two points to the front and back stagnation point of the cylinder and at the leading edge of the airfoil. At the rest of the grid points the deviation was less than 0.5 degrees. The orthogonal property of the current grid generating method was compared with the other grid generating methods available in literature. Comparison between the different methods is shown in Table.1. The deviation from orthogonality for the proposed SFC-based non-uniform grid appears to be comparable to other listed methods.

Table 1. Comparison of orthogonal property of different orthogonal grid generating system

Method	Maximum Departure (in degrees)	Geometry
Steger and Chausse[36]	16	Turbine blade
Duraiswamy and Prosperetti[37]	1.11	NACA 0015
Eca[38]	4.41	NACA 0015
Nair and Sengupta[39]	0.5	NACA 0015
Present	4-5	SD 7003/NACA 0012/NACA

3/13/2008

IV. Numerical Algorithm

The governing equations are discretized using high-order finite-difference schemes. This is done to reduce significantly the number of points required per wavelength compare to second-order schemes for the resolution of the acoustic waves and vortices[24].

A. Spatial Differences

A non-uniform compact scheme was proposed in Ref. 25. The scheme becomes identical to the uniform compact scheme proposed by Ref.24 .For some function f its derivative f' is computed as

$$\alpha_i f'_{i-1} + f'_i + \beta_i f'_{i+1} = \sum_{l=-2}^{2} A_{il} f_{i+l} \qquad (26)$$

The coefficients on the left-hand side and right-hand side can be obtained by matching the Taylor's series expansion. Close to the boundaries at $i=1$, 2 and $i= N-1$, N, the scheme is replaced with one-sided schemes and the coefficients are obtained accordingly. More details can be found in Refs. 14, 15. The value of α_i and β_i can be adjusted at each point but are kept constant at $1/3$ at each point and the scheme becomes central-differenced. On a non-uniform grid, the fourth-order accuracy is achieved.

B. Numerical filtering

Since the spatial differencing scheme is central-difference, numerical instabilities arising due to unresolved scales and grid non-uniformities can grow. Hence the solution is filtered according to the procedure suggested in Ref. 16. If f is the unfiltered solution and $\hat{f}$ is the filtered solution then

$$\alpha_f \hat{f}_{i-1} + \hat{f}_i + \alpha_f \hat{f}_{i+1} = \sum_{l=-5}^{5} a_{il} f_{i+l} \qquad (27)$$

Here α_f is a free parameter with values between -0.5 and 0.5 based on analysis using transfer function. The higher the value, the less dissipative is the filter. In the current study the value is set equal to 0.45. Since the stencil is wide, one-sided differencing formulas are needed at points (1... 5) and (N-4... N). Higher-order one-sided[26] formulas can be used to obtain the filtered values close to the boundaries. Ref 26 has a detailed discussion on the derivation and the order of the filters. The numerical filter employed in the current study is the tenth-order accurate.

C. Time Marching

Low-storage Runga-Kutta proposed by Ref.27 is used for marching the solution in time. The method is explicit and third-order accurate. The time marching for a system given by $df/dt=u$ is computed from time step m to time step m+1 as follows

$$f^{n+1} = f^n + b^{n+1} H_n \qquad (28)$$

$$H_n = a_n H_{n-1} + dtu, \qquad (29)$$

where n refers to the stage number. The value of f at the final stage of the scheme becomes the value at the timestep $m+1$. The values of the coefficients a_n and b_{n+1} have been given in Ref.27.

D. Boundary Conditions

Different kinds of boundary conditions have to be specified for the Euler and Navier Stokes equations. For Euler equations at the wall, ghost point boundary condition of Tam and Dong[28] in employed. No-slip boundary conditions are used for the stationary Navier-Stokes equations and the surface velocity components are set to the grid speed for the moving grid case. At the artificial domain boundary energy transfer and annihilation (ETA)[29] is employed with extrapolation of the values to domain boundaries.

V. Numerical Results

A. Euler Solver

As a first step, the code is validated for non-linear and linearized Euler equations (Eq.2, without the viscous terms) for curvilinear geometries using the SFC. A problem from the 2nd CAA workshop[40] is considered. The configuration describes the scattering of an initial acoustic pulse from a circular cylinder (See Fig.5a).The initial acoustic pulse is given by

$$p = p_\infty + 0.01 e^{\frac{-\ln(2)((x-x_c)^2+(y-y_c)^2)}{0.04}} \tag{30}$$

The center of the pulse (x_c, y_c) is located at (4,0). The domain is kept uniform in the region $[-8*8]*[-8*8]$ and coarsened beyond that with a stretching factor of 1.2. The results were computed on 300*300 and 450*450 grids and the results were found to converge. The pressure contour for pulse reflection from the cylinder and propagation into region of grid stretching are shown in Figs.6a, b. As can be seen in Fig.6b, the grid stretching and filtering absorbs the outgoing energy without producing non-physical

Final report FA9550-07-1-0314   3/13/2008

reflections back into the domain. The results are compared on different grids at P1 (0, 0.6) (Fig.5b). The results obtained on the 300*300 and 250*250 grid agreed with each other. For the 200*200 grid, two sets of computations were performed. It can be clearly seen from Fig.5b, the computations with clustering of grid points provides a closer match with the results obtained on the two previous grids. For the case with no grid clustering because of the coarse grid cells near the stagnation point, the number of grid points per wavelength is reduced. This causes smearing of the acoustic pulse. The clustering increases the number of points close to the stagnation region and ensures that sufficient numbers of points are present to resolve the waves.

Two different kinds of grid generation were mentioned in Section III.C for problems involving multiple bodies. To test the grid generation algorithm for multiple bodies using both the grid generation methods, sound scattering from two cylinders placed in tandem is considered (Fig.4). An initial pressure pulse is similar to the single cylinder case(Eq.30) and is located at the origin. The aeroacoustic computations were performed with the left cylinder of diameter 1 located at (-4, 0) and the right cylinder of diameter 0.5 located at (4, 0).The domain of computation is [-8, 8]*[-5, 5]. The acoustic pressure was monitored at the point (0, 2). As shown in Fig.7a excellent agreement is obtained between both methods of grid generation.

To test the long term stability of the solver and the boundary conditions, the scattering of periodic pulse placed from two cylinders in tandem is considered[41]. The aeroacoustic computations were performed with the same two cylinder tandem configuration but only on the stitched grid. A periodic source given by

$$S = 0.01e^{\frac{-\ln(2)((x-x_c)^2+(y-y_c)^2)}{0.04}} \sin(\omega t) \qquad (31)$$

was located at (0, 0).The value of w was taken to be 8π. The periodic source was added to the right-hand side of the energy equation and continuity equation. The initial values of the acoustic pressure and

velocities were assumed to be zero. The region close to the cylinder surface was stretched using a clustering parameter $\tau = 1$ in Eq. (22). The degree of stretching was kept limited to ensure at least 8 points per wavelength in the far field. The computations were performed on the 720*720 grid. The pressure history at a probe point is shown in Fig.7b and it can be seen that once the transient waves leave the domain, the solution has become periodic. The rms value of pressure was compared on the surface of the left (Fig.8a) and right cylinder (Fig.8b) with the analytical solution[41]. Very good match is obtained for both the cases and demonstrates the accuracy of computation for complex geometries.

B. Navier-Stokes Solver in Fixed Coordinates

To test the Navier-Stokes solver on stationary grids, the problem of uniform flow past a circular cylinder is considered first (see Figs. 9-10). This test case was chosen since abundant experimental and computational data are available for comparison of shed vortex pattern in the literature. It has been found that the vortex shedding appears for Re around 40-50 as observed in[32] and the references mentioned therein. Below the value of Re equal to 40, a pair of symmetric vortices is formed in the wake of the cylinder. The size of the vortices increases with Re until a value of Re=50 is reached, when the periodic vortex shedding begins.

All the simulations were performed with the grid sizes of 100*100, 150*150 and 200*200.The results obtained with the 150*150 and 200*200 grids are coincided. To resolve the viscous boundary layer, grid stretching was employed by adjusting the parameters P and Q to provide at least 15-20 points in the boundary layer. It was found that for the cases considered no grid clustering was needed in the φ direction.

The computations were performed at Re=20, 40,100 and 150. Table 2 presents a comparison of the current simulations and the available data. Good agreement is found at these Reynolds numbers. For the Re=20 and Re=40 (Figs.9b, c), steady symmetric vortices are formed behind the cylinder. The size of the vortices was compared with the available data from literature[32]. For the cases of Re=100 and 150, once

the transient flow leaves the domain, periodic vortex shedding appears behind the cylinder. Table 2 compares the Strouhal number (St) for vortex shedding obtained in the current study with results that has been published in the literature. Again the good agreement is found in terms of the Strouhal number.

Reynolds's Number	Current Simulations	Literature [42]
20	L=0.92 a=0.34 b=0.42	L=0.91-0.93 a=0.33-0.36 b=0.43-0.46
40	L=2.13-2.28 a=0.71-0.76 b=0.59-0.6	L=2.15 a=0.7 b=0.6
100	St=0.167	St=0.16-0.17
150	St=0.181	St=0.18-0.187

Table 2. Comparison of the vortex patterns between current simulation and data available in the literature

To test the Navier-Stokes solver in the range of moderate Reynolds numbers (10000-60000), uniform flow past a stationary airfoil (SD 7003) was studied at a Re=20000 over a range of angle of attacks (0-12 degrees). It was found that using the very mild value of grid clustering parameter $\tau=0.1$ the computed natural frequency of vortex shedding ($f=11.5$) was close to the measured frequency of vortex shedding ($f=12-13$).

C. Navier-Stokes Solver in moving coordinates

The aerodynamics of a plunging airfoil with $Re = \dfrac{U_\infty c}{\upsilon} = 20000$ was studied as a test case for the Navier-Stokes solver on the moving grid. The simulations were performed for NACA 0012 airfoil and SD 7003 airfoil.

The plunging motion of an airfoil is given by

$$y(t) = h\cos(2kt) \qquad (32)$$

where h is the plunging amplitude normalized by the chord length and $k = \dfrac{\omega c}{2U_\infty}$ is the reduced frequency. The NACA 0012 airfoil case was run for the Strouhal number St=kh=0.3. The computations were performed on four grid levels (G1 (240*80), G2 (300*80), G3 (360*80) and G4 (400*800)). The grids G3 and G4 were generated with grid clustering parameter $\tau = 1$ in Eq. (22). The G2 was generated with the grid clustering parameter $\tau = 2.0$ in Eq. (22). After an initial transient period of 2 cycles, the results become periodic. The results on G3 and G4 coincide while the results on G1 showed smearing. Peak coefficient of lift obtained using different grids (G2 and G3) and the results of Young[43] are shown in Fig.11. The obtained computational results correspond to those of Young[43] for the wide range of k.

The aerodynamics of a plunging SD 7003 airfoil were performed for two sets of data (i) h=0.025, k= 7.85 (St=0.196) and (ii) h=0.1, k = 5.91 (St=0.591). The former case is designated as a low Strouhal number case and the latter case is a high Strouhal number case. The grid speed y_τ is calculated from Eq.32. The computations were performed using G2 and G2 with $\tau = 3.5$. It was found that for the low St case the computations ran on both grids without producing any unphysical reflections. For the high St case, the computations with mild clustering produced large amounts of unphysical oscillations close to the leading edge which contaminated the solution. To remove the unphysical oscillations, the clustering parameter was changed to 3.5 and the unphysical oscillations were avoided. For high St, strong leading edge vortex is observed as shown in Fig.12.

The flow field was compared with the flow visualization of OI[44] for both the cases by plotting the hyperbolic tangent of vorticity. Similar vorticity pattern to the experiments were observed during the top stroke and bottom stroke (Fig.13) showing the accuracy of the computations.

VI. Gust Suppression by Flapping Airfoils

In the current study, the effect of the wind gust on the aerodynamic performance of a 2D plunging airfoil is examined numerically using a Navier-Stokes solver in moving coordinates described above. The gust is included as a source term[45] in the right-hand side of the momentum equations to avoid dealing with the numerical problems to propagate gust at the boundaries of the computational domain. The flight of Micro Air Vehicles (MAV) experiences high unsteady flow conditions due to the gusty winds in the atmosphere. Birds and insects, which operate under similar conditions, use the flapping motion of their wings to generate thrust and lift. To improve the design of the MAV to suit the operating conditions, a number of studies have been performed to study the aerodynamics of insects and simplified models of airfoils. However, the effect of the wind gust, which is a very important factor in the MAV design, has been neglected in most of these studies. In the current study, the effect of the wind gust on performance of MAV and the ability to suppress the effect of wind gust using the plunging motion of the airfoil is examined.

The gust is included as a source term in the right-hand side of the momentum equations to avoid dealing with the problems at the boundaries of the computational domain:

$$S = \begin{pmatrix} 0 \\ C_1 \cos(kt) \\ C_2 \cos(kt) \\ 0 \end{pmatrix},$$

where k is the reduced frequency given by $k = \dfrac{wc}{2U_\infty}$. The coefficients C_1, C_2 are given by

$$C_1 = 3a(1 + \cos(b(x - x_c)))(\tanh(3(y + y_c))^2 - \tanh(3(y - y_c))^2) \quad (33)$$

3/13/2008

$$C_2 = ab\sin(b(x - x_c)))(\tanh(3(y + y_c)) - \tanh(3(y - y_c))) \qquad (34)$$

in the range $|x - x_c| \le \dfrac{\pi}{b}$ and 0 for other values, a represents the gust amplitude, b represents the gust

width, x_c, y_c represent the center of the vortical gust.

The amplitude of plunging (h) is computed from the formula

$$h = \varepsilon \max(C_1, C_2), \qquad (35)$$

where ε is a parameter, which is used to adjust the plunging amplitude to match the lift force

generated by the vortical gust with the lift force generated by the plunging motion of airfoil.

Computations were performed for three cases: (plunging frequency and the vortical gust frequency

were equal)

- o Stationary airfoil with vortical gust (Case 1)

- o Plunging airfoil with no vortical gust (Case 2)

- o Plunging airfoil used to suppress the oscillatory lift force created by the vortical gust.(Case 3)

The comparisons are shown in Fig.14 for $a = 0.8, b = 5, h = 0.007, k = 3.93$. As the gust propagates with

the mean flow, the approximate non-dimensional wavelength of the gust is 0.8. As the non-dimensional

chord length of the airfoil in the computation is equal to unity, more than one wavelength of the gust is

swept across the airfoil during each instant. The computations for case 1 and case 2 in Fig.1 shows that

the case 1 and case 2 are approximately out of phase. For the case 3, it is found that lift suppression has

been achieved but the suppression is not a simple superposition of the lift force generated due to the gust

and the plunging motion. For more exact cancellation of the gust lift, the pure plunging should be

combined with the pitching motion of airfoil that will be considered in our future research.

VII. Conclusions

Streamline as a Coordinate method (SFC) was used in the past for steady aerodynamics with low-

order of approximation of governing partial differential equations. The advantages of the SFC are the

3/13/2008

ability of grid to adhere to the curvilinear airfoil surface, to resolve the boundary layer, and to move with the pitching and plunging airfoil. The use of SFC for aerodynamics of flapping airfoils was hindered by low accuracy of the SFC method near stagnation points.

In the current study the SFC method using analytical and numerical solutions of potential function and patching of sub-domains was combined with the high-order spatial and temporal discretizations in a single-grid approach. The far-field SFC grid approaches Cartesian grid so the ETA method was found to absorb the outgoing numerical error. The presented results show the orthogonality property of the grid generated. This paves the way to adopt the economic single-grid approach for complex geometry when high-order schemes are needed. However, it was observed that a uniform distribution of SFC grid points in the computational domain produces coarse grid cells close to the stagnation point that may harm the effort of utilization of high-accuracy high-order schemes. To circumvent this issue, a sine hyperbolic stretching function was used for grid refinement in the φ direction in the current study.

The numerical solution of governing Navier-Stokes in non-inertial coordinates have shown that the non-clustered grid in the φ direction in the vicinity of stagnation points can be used if the modeled flow is steady, that is, the only velocity scale is present and this velocity tends to zero near the stagnation point. If another non-zero velocity scale is present such as the speed of flapping airfoil, the grid clustering is needed in the φ direction in the vicinity of stagnation points.

The scattering of sound from single and multiple cylinders was taken as representative cases for which analytical or well-established numerical solutions are available for inviscid Euler equations. For the case of a single cylinder and multiple cylinders, the computed acoustic pressure matched well with the exact solution when appropriate clustering of grid points is implemented. Uniform flow past a single cylinder was taken as a test case for viscous flows at low Reynolds numbers. The size of shed vortices for this case had a good agreement with the data available in the literature. For the periodic shedding at Re=100 and 150, the Strouhal number matched with the values given in the literature. The grid refinement in the φ direction in the vicinity of stagnation points was not needed since the only velocity scale is present.

Final report FA9550-07-1-0314   3/13/2008

The vortex shedding from a SD 7003 airfoil in uniform flow was studied as a test case for moderate Reynolds number flow (Re=20000) and it was found that the computed natural shedding frequency agreed well with the experimental results with very mild grid clustering in the φ direction.

Plunging of airfoils at two different Strouhal numbers was studied to find the necessary degree of grid clustering near stagnation points. The measured coefficient of lift for the case of NACA 0012 airfoil coincided with the results obtained by Young[43]. The flow field visualization for SD 7003 plunging airfoil showed similar structures to the observed experimental pattern when appropriate clustering of grid points in the φ direction is implemented. Further, it was found that the amount of grid clustering required in the ϕ direction increased for higher Strouhal numbers, that is, for a higher plunging speed of the moving airfoil.

Acknowledgments

References

[1]Von Mises, R, "Bemerkungen zur Hydrodynamik", *ZAMM*, Vol. 7, 1927, pp.125

[2]Barron, R. M., An, C. F. and Zhang, S., "Survey of the streamfunction-as-a-coordinate method in CFD", *Proc. of the Inaugural Conference of the CFD Society of Canada*, Montreal, Canada, June,1993, pp. 14-15

[3]Hui, W.H and Loh, C.Y, "A new Lagrangian method for steady supersonic flow computation. Part 1.Gudunov scheme", *Journal of Comp. physics*, Vol.89, 1990, pp.207-240

[4]Loh, C.Y and Liou, M.S., "A new Lagrangian method for solving 3-D steady supersonic flow problem", *Proc. of 1ˢᵗ European CFD Conference*, Brussels, Belgium, Sept. 7-11, 1992

[5]Loh, C.Y and Liou, M.S., "Computing 3-D steady supersonic flow via a new lagrangian approach", *AIAA paper 93-0891*, 1993

[6]Martin, M. H., "A new approach to problems in two dimensional flow", *Quart. J. Appl. Math.* , Vol. VIII, No.2, 1950, pp.137-150

[7]Martin, M. H., "The flow of a viscous fluid", *Archives for Rational Mechanics and Analysis*, Vol. 41, 1971, pp.266-298

[8]Osipov,I.L.,Shiplin,A.V. and Shulishnina, N.P, "A numerical method for calculation of gas flows in channels and nozzles in direct, inverse and combined modes",*Zh.Vychisl. Mat. I Mat. Fiz*, Vol.27, No.10, 1987, pp. 1563-1572(in Russian)

[9]Barron, R.M., "A non-iterative technique for design of airfoils in incompressible potential flow", *Comm. Appl. Num. Methods*, Vol.6, 1990, pp. 557-564

[10]Barron, R.M. and An, C.-F., "Analysis and design of transonic airfoils using streamline coordinates", *Proc. 3ʳᵈ Intl. Conf. on inverse design concepts and optimization in Eng.Sci.*, Washington, DC, USA, ed. By G.S. Dulikravich, 1991, pp. 359-370

[11]Finnigan,J.J, "A streamline coordinate system for distorted two-dimensional shear flows", *Journal of fluid Mechanics*, Vol.130, 1983, pp. 241-258

[12]Finnigan, J.J, *Streamline Coordinates, Moving frames, Chaos and Integrability in Fluid Flow*, In Topological Fluid Mechanics, Cambridge University Press, 1990

[13]Finnigan, J.J and Bradley, E.F., "The turbulent kinetic energy budget behind a porous barriers: An analysis in streamline co-ordinates", Journal of Wind Eng. And Ind. Aerodyn., Vol. 15, 1983, pp. 157-168

[14]Barron, R.M., Zhang, S., Chandna, A. and Rudraiah, N., "Axisymmetric potential flow calculations Part 1: Analysis mode", *Comm. Appl. Num. Methods*, Vol.6, 1990, pp. 437-445

[15]Hamdan, M.N and Barron, R.M, "Applications of von mises coordinates in porous media flow", *Journal of Comp. applied Math.*, Vol.39, 1992, pp. 353-361

[16]Chakravarthy, S. R., "Inviscid analysis of dual-throat nozzle flows", *AIAA, Fluid and Plasma Dynamics Conference*, 14th, Pao Alto, CA, 23-25 June 1981,

[17]Adamczyk, J. J., "An electrostatic analog for generation cascade grids", N81-14690 05-64, 1980

[18]Symm, G. T., "An integral equation method in conformal mapping", *Numerische Mathematik*, Vol. 9, No.3, 1966, pp. 250-258

[19]Anderson, O.L and Hankins Jr., G.B., "Development of a parabolic finite difference method for 3-D high Reynolds number viscous internal flows", *Computers in flow prediction and Fluid dynamic Experiments, ASME*, Washington, D.C., 1981, pp. 119

[20]Briley, W. R., "Analysis and computation of viscous primary and secondary flows", *Computational Fluid Dynamics Conference*, Williamsburg, Va., American Institute of Aeronautics and Astronautics, Inc., July 23-25, 1979, p. 74-88

[21] Hounjet, M. H. L., "Hyperbolic Grid Generation with BEM Source terms", NLR TP 90334, 1990

[22]Hounjet, M. H. L., "Hyperbolic Grid Generation control by panel methods", NLR TP 91061, 1991

[23]Anderson, D. A., Tannehill, J. C. and Pletcher, *R. H., Computational Fluid mechanics and heat transfer*, 2nd edition, McGraw-Hill Book Co., 1984,

[24]Lele, S. K., "Compact finite difference scheme with spectral like resolution", *Journal of Computational Physics*, Vol. 103, No.1, 1992, pp.16-42

[25]Gamet, L., Ducros, F., Nicoud, F. and Poinsot, T., "Compact finite difference schemes on non-uniform meshes. Application to direct numerical simulations of compressible flows", *Intl. Journal for Num. methods in fluids*, Vol .29, No. 2, 1999, pp.159-191

[26] Visbal, M. R. and Gaitonde, D. V., "Very High-Order Spatially Implicit Schemes for Computational Acoustics on Curvilinear Meshes", *Journal of Computational Acoustics*, Vol. 9, No. 4, 2001, pp. 1259-1286

[27] Williamson, J. H., "Low-storage Runga-Kutta schemes", *Journal of Computational Physics*, Vol. 35, 1980, pp. 48-56.

[28] Tam, C. K. W and Dong, Z., "Wall boundary conditions for high-order finite difference schemes in computational aeroacoustics", *Theoretical and Computational Fluid dynamics*, Vol. 6, 1994, pp. 303-322.

[29] Edgar, N. , Visbal, M. R.,, "A General Buffer Zone-type Non-Reflecting Boundary Condition for Computational Aeroacoustics", *9th AIAA/CEAS Aeroacoustics Conference and Exhibit*, Hilton Head, South Carolina, May 12-14, 2003, AIAA-2003-3300

[30] Steger, J. L., "Implicit Finite Difference simulation of flow about arbitrary geometries with application to airfoils", 10th Fluid *and Plasmadynamics Conference*, Albuquerque, N. Mex., June 27-29, 1977, AIAA-1977-665

[31] Katz, J. and Plotkin, A, *Low-Speed Aerodynamics*, Cambridge Aerospace Series, 1991

[32] Thompson, J. K., Warsi, Z.U.A. and Mastin, C. W., *Numerical grid generation: foundations and applications*, Elsevier North-Holland, Inc. New York, NY, USA, 1985

[33] Knupp, P. M. and Steinberg, S., *The Fundamentals of Grid Generation*, 1st edition, CRC Press, 1993

[34] Vinokur, M., "On One-dimensional Stretching Functions for Finite-difference Calculations", NASA-CR-3313, 1980

[35] Fletcher, C. A. J., *Computational Techniques for Fluid Dynamics. Specific Techniques for Different Flow Categorie*s 2nd edition, Springer-Verlag, 1991

[36] Steger, J.L. and Chaussee, D.S., "Generation of Body-Fitted Coordinates Using Hyperbolic Partial Differential Equations", *SIAM Journal on Scientific and Statistical Computing*, Vol.1, No.4, 1980, pp. 431-437

[37] Duraiswami, R. and Prosperetti, A., "Orthogonal mapping in two dimensions", *Journal of Computational Physics*, Vol.98, No.2, 1992, pp.254-268

[38]Eca, L., "2D Orthogonal Grid Generation with Boundary Point Distribution Control", *Journal of Computational Physics*, Vol.125, No.2, 1996, pp.440-453

[39]Nair, M. T. and Sengupta, T. K., "Orthogonal grid generation for Navier-Stokes computation", *International Journal for Numerical Methods in Fluids*, Vol.28, No.2, 1998, pp. 215-224

[40]Tam, C. K. W. and Hardin, J. C., "Second Computational Aeroacoustics CAA Workshop on Benchmark Problems", NASA CP-3352, 1997

[41] Dahl, M., D., "Fourth Computational Aeroacoustics CAA Workshop on Benchmark Problems", NASA CP-2004-212954, 2004

[42]Linnick, M.N. and Fasel, F. H, "A high-order immersed interface method for simulating unsteady incompressible flows on irregular domains", *Journal of Comp. Physics*, Vol.20, No.1, 2005, pp. 157-192

[43]Young, J., "Numerical simulation of unsteady aerodynamics of flapping airfoils", Ph.D. dissertation, School of Aerospace, Civil and Mechanical Engineering, The University of New South Wales

[44]Ol, M., "Vortical Structures in high frequency pitch and plunge at low Reynolds numbers", *37th AIAA Fluid Dynamics Conference and Exhibit*, 25 - 28 June 2007, Miami, FL , AIAA2007-4233

[45]Lockard, D. P. and Morris, P. J., "Radiated noise from airfoils in realistic mean flows", AIAA Journal, Vol.36, No.6, 1998, pp. 907-914
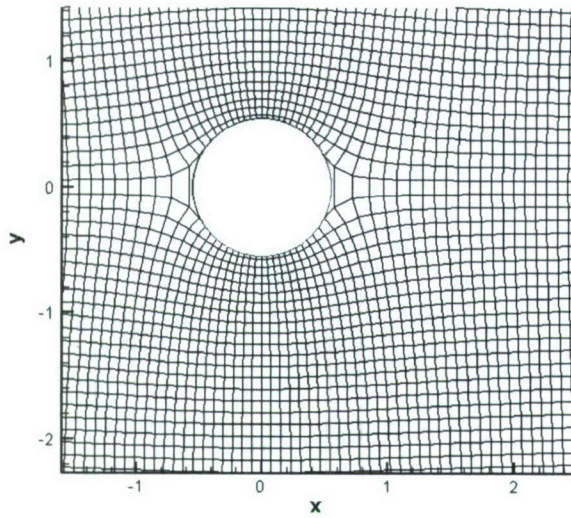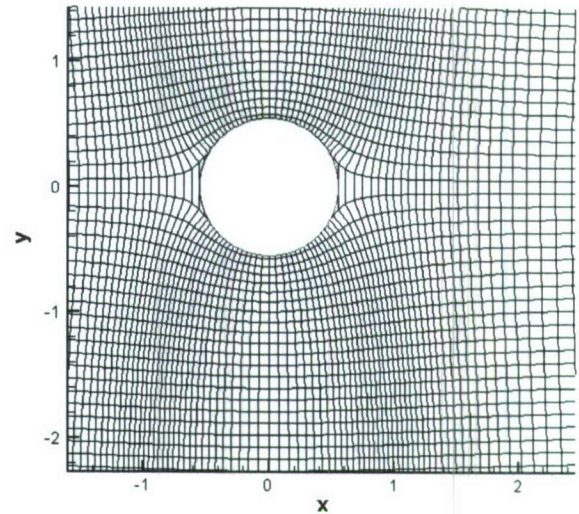
(a)   (b)

Figure 1. The SFC grid around a cylinder: (a) uniform grid and (b) grid stretching in the φ-direction close to the stagnation points.(τ=4, in Eq. (22))
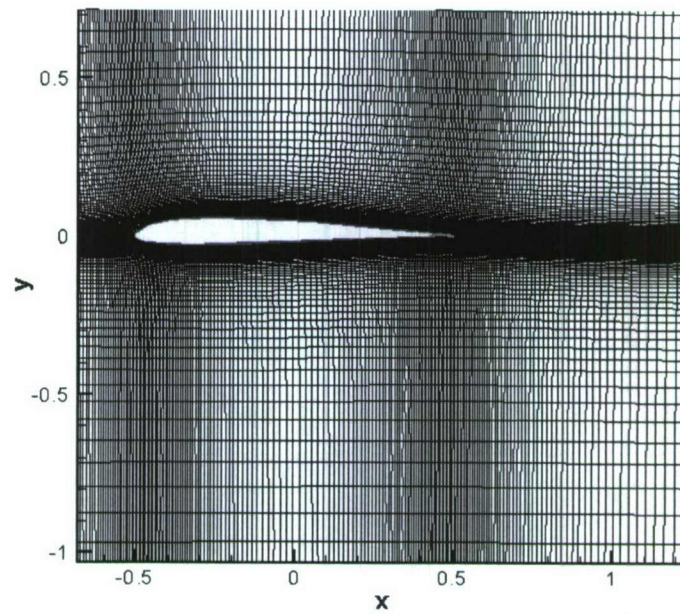
Figure 2. Grid generated using panel method for SD 7003 Airfoil: Domain with boundary layer ψ-clustering and the φ-clustering close to stagnation point
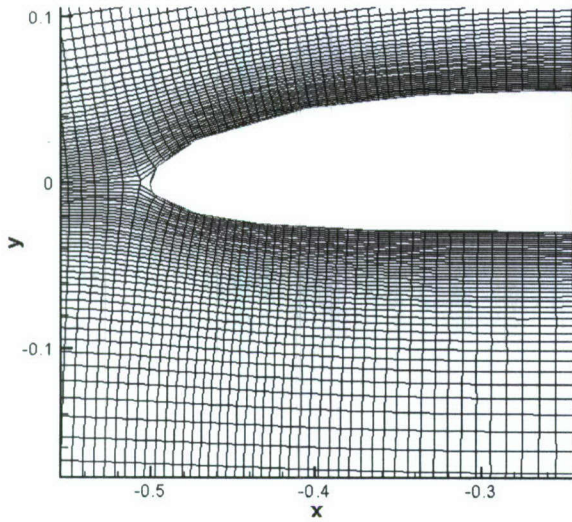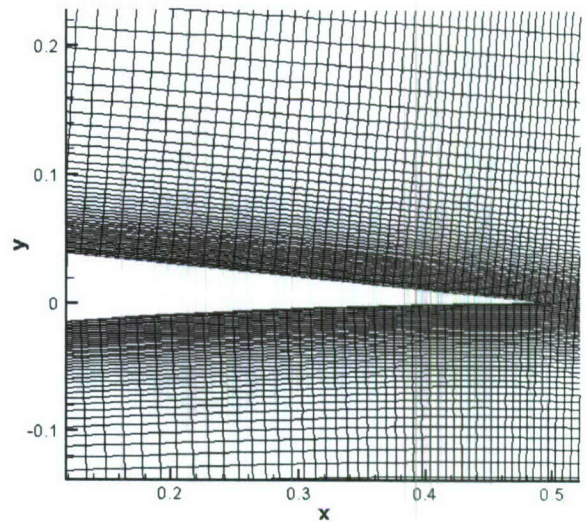
(a)   (b)

Figure 3. Grid generated using panel method for SD 7003 Airfoil: (a) zoomed-in view of leading edge and (b) zoomed-in view of trailing edge
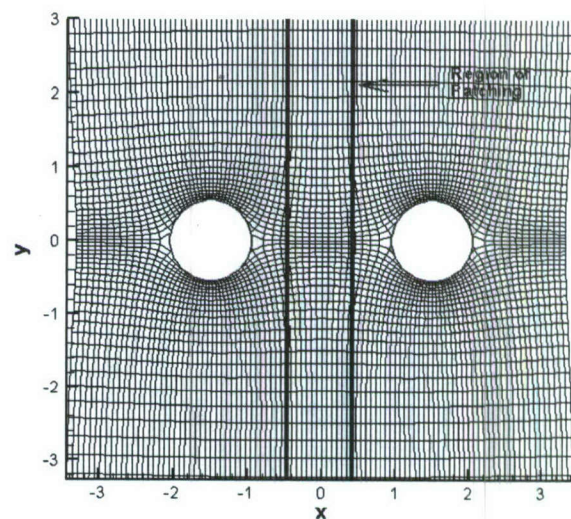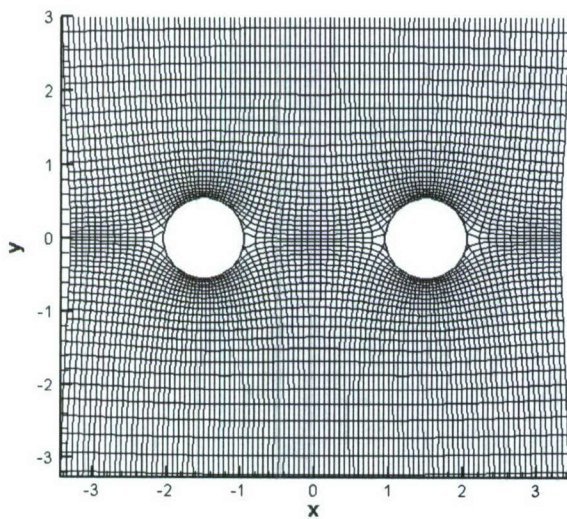
Figure 4. Grid generation for pair of cylinders in tandem: (a) using panel method solution of two cylinder system and (b) local panel method solution for each cylinder followed by stitching along the region of patching. Every second grid line is shown on either side starting from the streamline on top and bottom of the cylinder for both the cases.

(a)

(b)
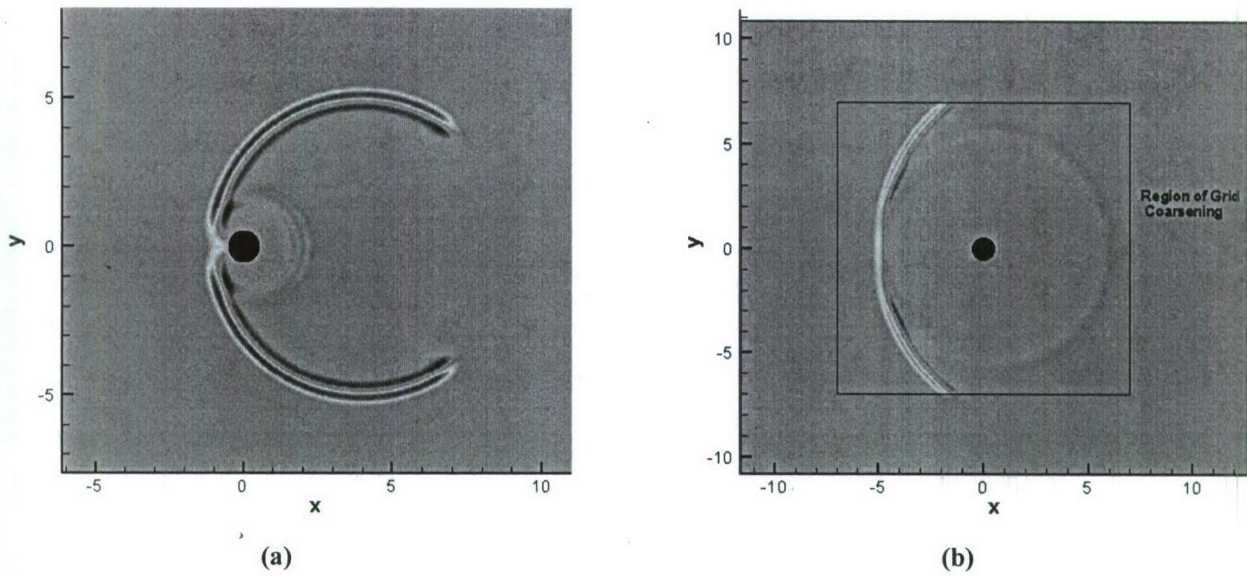
Figure 5. Pressure contour for scattering of an initial pulse from cylinder a) t=5 and b) t=9.

(a)

(b)
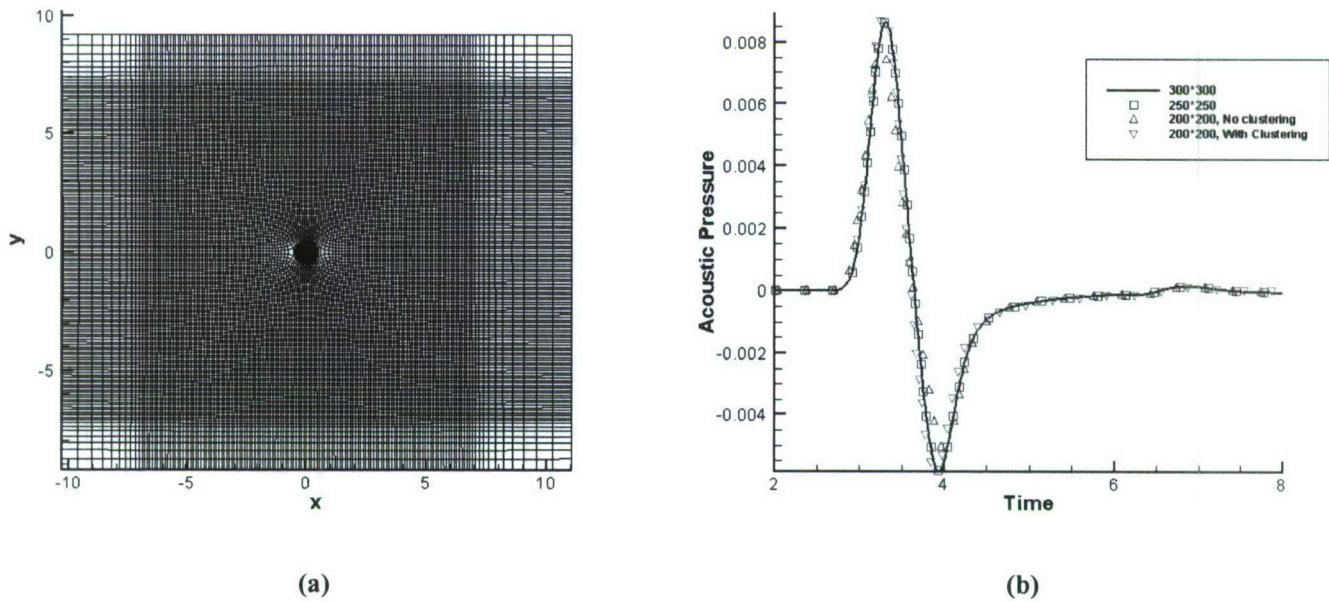
Figure 6.Results on the scattering of acoustic pressure from a single cylinder: (a) numerical grid with coarsening and (b) acoustic pressure at P1 obtained by using a uniform grid (300*300) and a grid of 200*200 with and without clustering close to stagnation point

3/13/2008
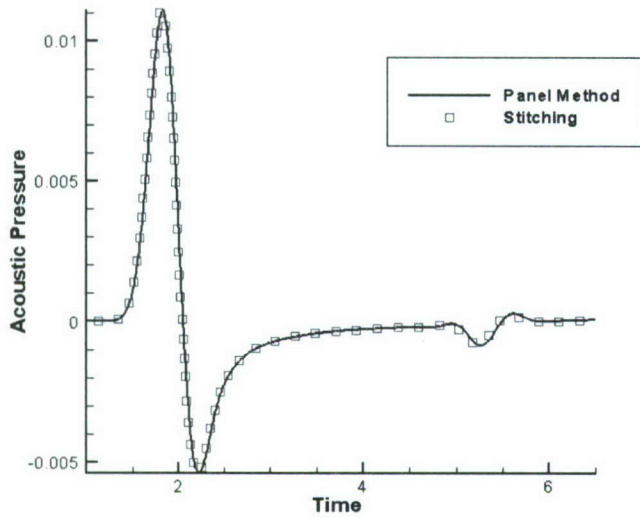
(a)
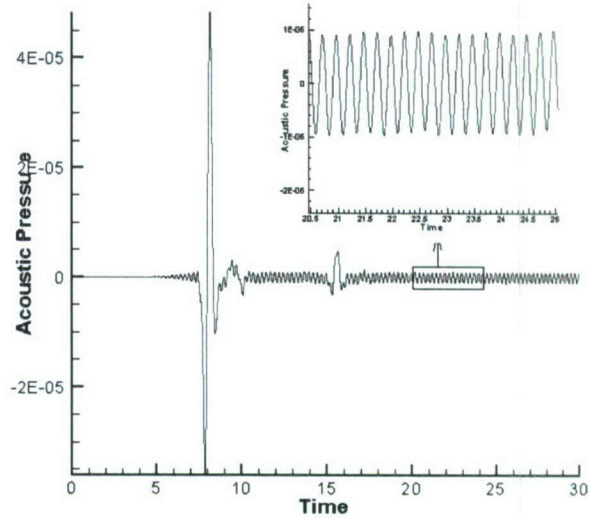
(b)

Figure 7. Sound scattering from the pair of cylinders: (a) momentarily acoustic pulse computed on grids obtained by grid stitching method and by the single-domain panel method and (b) pressure history at probe point for scattering of a periodic pulse
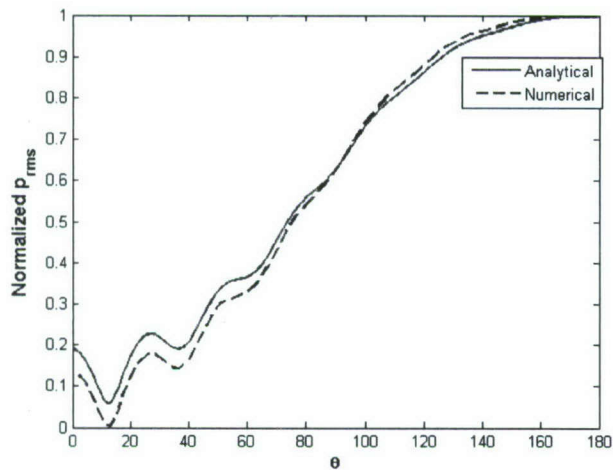
(a)
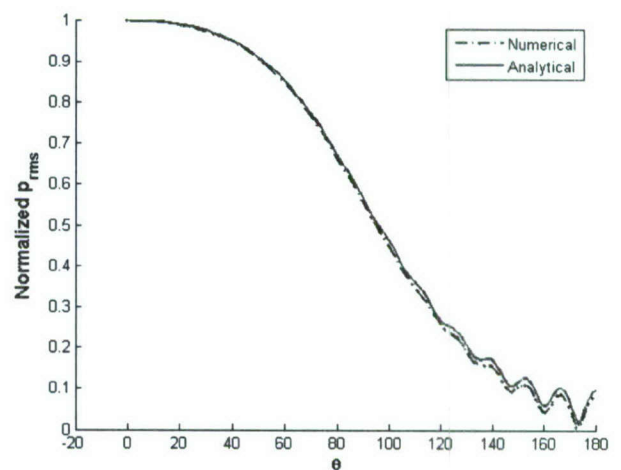
(b)

Figure 8.Comparison of analytical and numerical solutions for scattering of a periodic pressure pulse from the pair of cylinders: (a) acoustic pressure on the surface of the left cylinder and (b) Acoustic pressure on the surface of the right cylinder

(a)   **(b)**   **(c)**
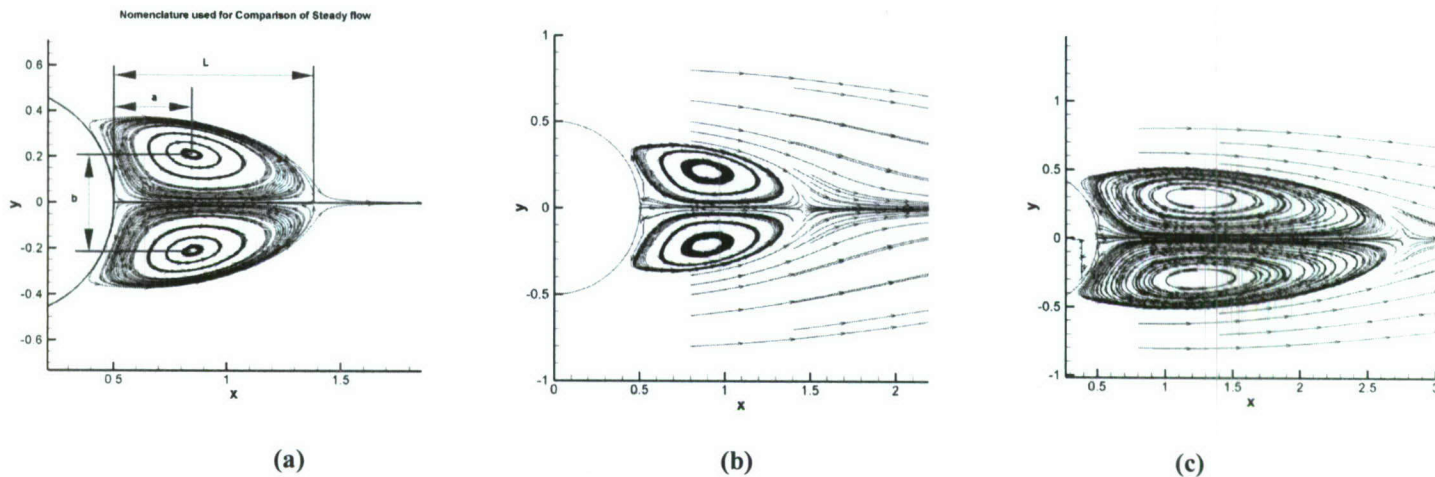
Figure 9. Steady vortex past a single circular cylinder: a) nomenclature used for comparing quantities of interest, b) Vortex pattern for Re=20, and c) vortex pattern for Re=40.

(a)   **(b)**
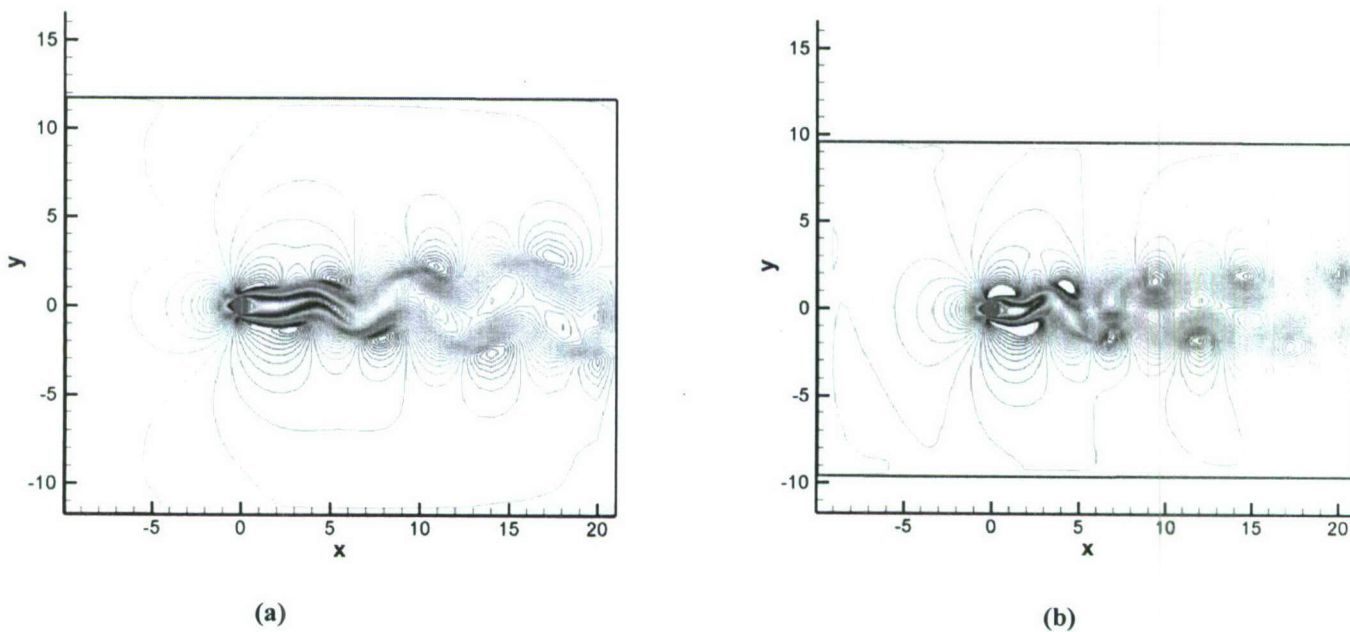
Figure 10. Shedding of street of vortices past a single cylinder: a) Re=100 and b) Re=150

Final report FA9550-07-1-0314   3/13/2008
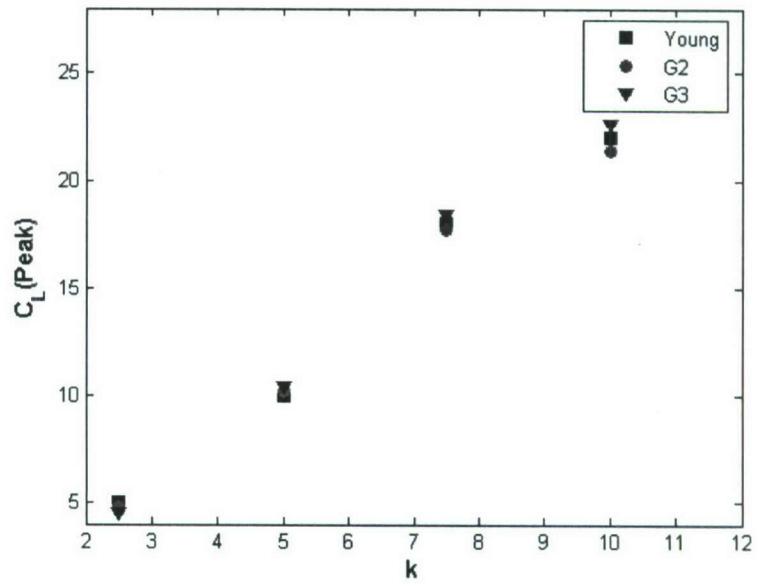
Figure 11. Peak coefficient of lift for plunging NACA 0012 airfoil

(a)

(b)
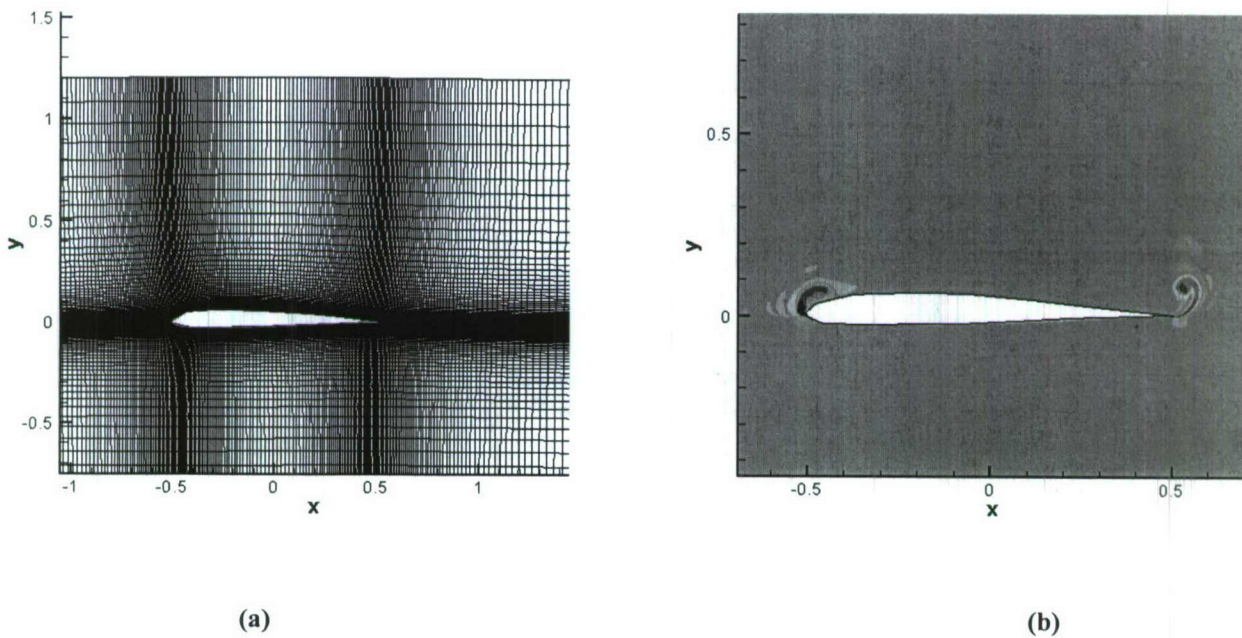
Figure 12. Plunging SD 7003 airfoil for St=0.591: (a) refined grid and (b) Isolines of hyperbolic tangent of vorticity
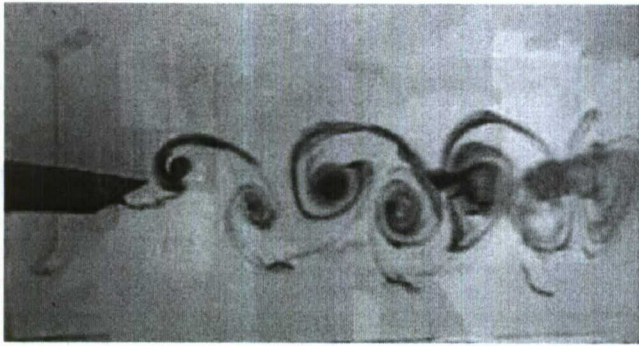
(a)
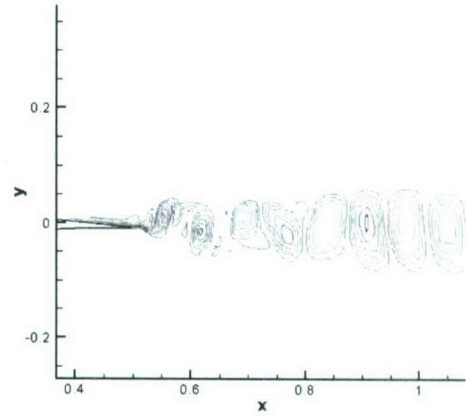
(b)
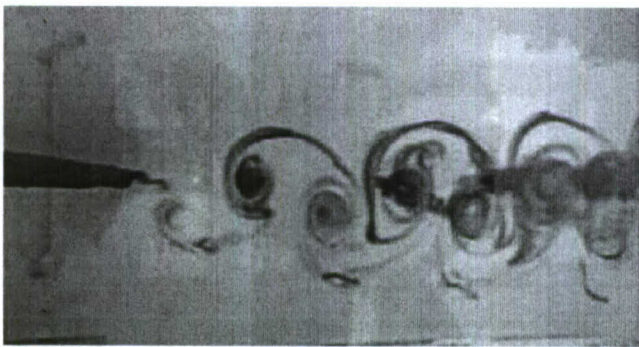
(c)
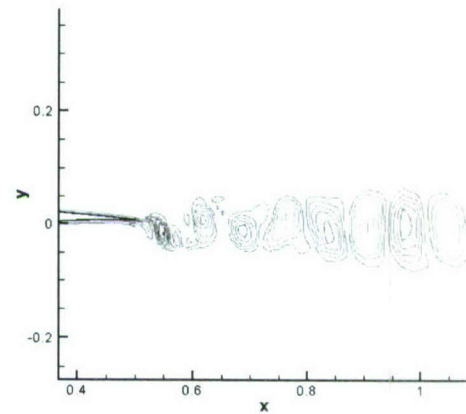
(d)

Fig.13 Comparison between experimental observation and numerical simulation for plunging SD7003, Case 1: (a-b) bottom stroke, (c-d) top stroke, (a, c)-experimental visualization, (b, d)-computational isolines of vorticity. Hyperbolic tangent of vorticity obtained by the numerical simulations is shown in subfigures (b, d)
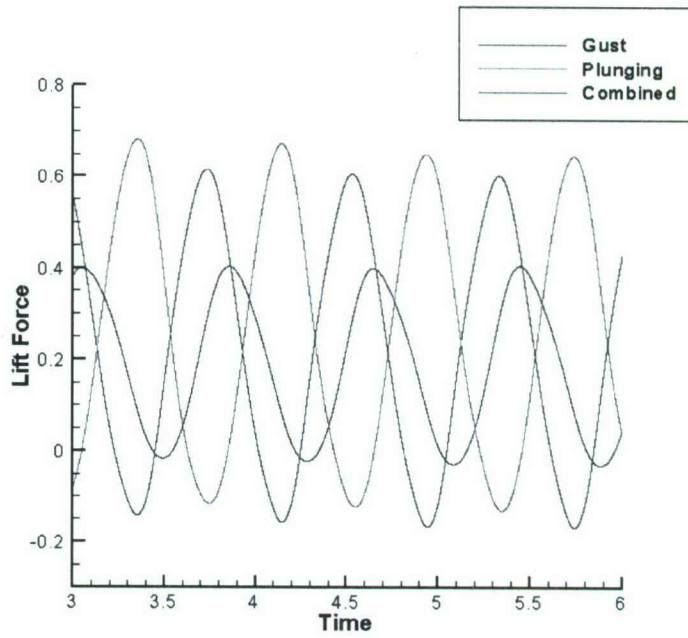
Figure 14. Comparison of the Lift force for the three cases: Case 1 (gust), Case 2 (plunging), and Case 3 (combined). In the Case 3, airfoil plunging suppresses the effect of gust.

Final report FA9550-07-1-0314   3/13/2008